

# Thermal Ignition

Thesis by

Philipp Andreas Boettcher

In Partial Fulfillment of the Requirements

for the Degree of

Doctor of Philosophy



California Institute of Technology

Pasadena, California

2012

(Defended May 2<sup>nd</sup> 2012)

© 2012

Philipp Andreas Boettcher

All Rights Reserved

To Leslie, Juliane, Jane, Helmut, Frank, & Trey

# Acknowledgments

I would like to acknowledge my advisor, Joseph Shepherd, first. It has been a great pleasure to work with him. He has put a tremendous amount of trust in me and his other students, as we perform combustion experiments. I am very grateful for the opportunity to work for him and very much enjoyed our discussions about science, engineering, history, and philosophy. Guillaume Blanquart has been my *de facto* co-advisor since joining the mechanical engineering faculty. His expertise in combustion and numerical simulation have been a great resource during my time. I am also very grateful to the other members of my thesis committee, Beverly McKeon and John Dabiri, for their help and insightful discussions.

I would also like to thank the other faculty members of GALCIT, particularly Tony Leonard, Dale Pullin, Dan Meiron, and of course Ravi and Hans Hornung for their help on my candidacy committee as well as their general encouragement.

None of this work would have been possible without the other group members of the Explosion Dynamics Laboratory and T5. Jim Karnesky taught me everything I know about electronics, building experiments (and making them work), and lab safety. Sally Bane and I worked closely under the funding provided by Boeing, which Stephanie Coronel is now continuing. An extra big thanks goes to Jason Damazo, “the smart one”, whose collaboration is invaluable. We worked closely on several projects, which are not part of this thesis, but made my graduate school experience much more enjoyable mainly because I got to work with Jason. His expertise in experiments, math, and coding have been a great help. Rémy Mével and Vaughan Thomas are the reason that the auto-ignition work has the current level of detail and made it publication. Both of them have been in the office during the final stages of the thesis writing process and helped me talk through a host of problems. Brian Ventura deserves a lot of credit for his help with the puffing flame investigation. He started with me as a SURF student and I convinced him to stay on and do a senior thesis. Our collaboration in the lab made the rather tedious experiments go by much more quickly. Kliulai Chow-Yee also did a SURF project in the lab and helped with the color schlieren pictures. Aurelien Demenay helped

with the very tedious manual digitization of the flame speeds from schlieren videos. Nick Parziale, who works in T5, is close friend and has kept me going for the past few year. Bahram Valiferdowski has been an excellent resource for all engineering design questions and group morale. Thanks also to Joe Jewell for taking over the 150 seminar and general group entertainment. Alexandra Katsas was a great help and support throughout the years. I would also like to thank Shannon Kao, and Neil Bitter and Bryan Schmidt for setting the stage and continuing the legacy respectively. Shyam Menon, who I would like to nominate as a honorary EDL member, performed all of the simulations for the puffing flame project and helped me try to unravel the phenomenon.

A special thanks goes to the Aeroshop, Brad St John, Ali Kiani, and Joe Haggerty. All of my experimental work was possible by the parts they fabricated, as well as the design help and encouragement I received.

My friends and roommates kept me sane during my time here: Chris, Angie, Pablo, Tony, Paco, Jason R., Travis, Olive, Veronica, and Dr. Jay.

Several members of the staff here at Caltech were exceptional during my stay here with help and opportunities to help others – a big thank you to Felicia, Natalie, Icy, and Kevin. Special thanks also to Dennis Kwon, Adam Savage, and Jamie Hyneman for the opportunity to work on Mythbusters. Jason and I had a wonderful time.

This work was made possible by The Boeing Company through the Strategic Research and Development Relationship Agreement CT-BA-GTA-1. In particular I would like to thank, Eddie Kwon and Art Day at Boeing with whom we worked closely, as well as Mike Grant, Debbie Raddash, and Matt Ganz for their support.

I would like to thank my family for all their support: my parents — Juliane and Helmut; my host family — Jane, Frank, and Trey; my grandparents — Margret and Ludwig; as well as all my aunts, uncles, and cousins. Thank you for cheering me on.

The final thanks is reserved for Leslie Lamberson, who made all of this worth while. I am looking forward to our future together.

# Abstract

Accidental ignition of flammable gases is a critical safety concern in many industrial applications. Particularly in the aviation industry, the main areas of concern on an aircraft are the fuel tank and adjoining regions, where spilled fuel has a high likelihood of creating a flammable mixture. To this end, a fundamental understanding of the ignition phenomenon is necessary in order to develop more accurate test methods and standards as a means of designing safer air vehicles. The focus of this work is thermal ignition, particularly auto-ignition with emphasis on the effect of heating rate, hot surface ignition and flame propagation, and puffing flames.

Combustion of hydrocarbon fuels is traditionally separated into slow reaction, cool flame, and ignition regimes based on pressure and temperature. Standard tests, such as the ASTM E659, are used to determine the lowest temperature required to ignite a specific fuel mixed with air at atmospheric pressure. It is expected that the initial pressure and the rate at which the mixture is heated also influences the limiting temperature and the type of combustion. This study investigates the effect of heating rate, between 4 and 15 K/min, and initial pressure, in the range of 25 to 100 kPa, on ignition of *n*-hexane air mixtures. Mixtures with equivalence ratio ranging from  $\phi = 0.6$  to  $\phi = 1.2$  were investigated. The problem is also modeled computationally using an extension of Semenov's classical auto-ignition theory with a detailed chemical mechanism. Experiments and simulations both show that in the same reactor either a slow reaction or an ignition event can take place depending on the heating rate. Analysis of the detailed chemistry demonstrates that a mixture which approaches the ignition region slowly undergoes a significant modification of its composition. This change in composition induces a progressive shift of the explosion limit until the mixture is no longer flammable. A mixture that approaches the ignition region sufficiently rapidly undergoes only a moderate amount of thermal decomposition and explodes quite violently. This behavior can also be captured and analyzed using a one-step reaction model, where the heat release is in competition with the depletion of reactants.

Hot surface ignition is examined using a glow plug or heated nickel element in a series of premixed

*n*-hexane air mixtures. High-speed schlieren photography, a thermocouple, and a fast response pressure transducer are used to record flame characteristics such as ignition temperature, flame speed, pressure rises, and combustion mode. The ignition event is captured by considering the dominant balance of diffusion and chemical reaction that occurs near a hot surface. Experiments and models show a dependence of ignition temperature on mixture composition, initial pressure, and hot surface size. The mixtures exhibit the known lower flammability limit where the maximum temperature of the hot surface was insufficient at igniting the mixture. Away from the lower flammability limit, the ignition temperature drops to an almost constant value over a wide range of equivalence ratios ( $0.7 < \phi < 2.8$ ) with large variations as the upper flammability limit is approached. Variations in the initial pressure and equivalence ratio also give rise to different modes of combustion: single flame, re-ignition, and puffing flames. These results are successfully compared to computational results obtained using a flamelet model and a detailed chemical mechanism for *n*-heptane. These different regimes can be delineated by considering the competition between inertia, i.e., flame propagation, and buoyancy, which can be expressed in the Richardson number.

In experiments of hot surface ignition and subsequent flame propagation a  $\sim 10$  Hz “puffing” flame instability is visible in mixtures that are stagnant and premixed prior to the ignition sequence. By varying the size of the hot surface, power input, and combustion vessel volume, we determined that the instability is a function of the interaction of the flame with the fluid flow induced by the combustion products rather than the initial plume established by the hot surface. The phenomenon is accurately reproduced in numerical simulations and a detailed flow field analysis revealed a competition between the inflow velocity at the base of the flame and the flame propagation speed. The increasing inflow velocity, which exceeds the flame propagation speed, is ultimately responsible for creating a puff. The puff is then accelerated upward, allowing for the creation of the subsequent instabilities. The frequency of the puffing is proportional to the gravitational acceleration and inversely proportional to the flame speed. We propose a relation describing the dependence of the frequency on gravitational acceleration, hot surface diameter, and flame speed. This relation shows good agreement for lean and rich *n*-hexane-air as well as lean hydrogen-air flames.

# Contents

<b>Abstract</b>	<b>vi</b>
<b>List of Figures</b>	<b>xxv</b>
<b>List of Tables</b>	<b>xxvii</b>
<b>1 Introduction</b>	<b>1</b>
1.1 Motivation . . . . .	1
1.2 Background . . . . .	3
1.2.1 Thermal Ignition in a Heated Vessel — Auto-Ignition . . . . .	5
1.2.2 Thermal Ignition from a Concentrated Hot Surface . . . . .	8
1.2.3 Hot Surface Ignition of Liquid Fuels . . . . .	10
1.2.4 Cyclic Flame Propagation in Premixed Combustion . . . . .	10
1.3 Thesis Outline . . . . .	12
<b>2 Thermal Ignition of Gaseous Fuel-Air Mixtures Within a Slowly Heated Vessel</b>	<b>13</b>
2.1 Introduction . . . . .	13
2.2 Experiments . . . . .	14
2.2.1 Experimental Setup . . . . .	14
2.2.2 Experimental Results . . . . .	16
2.2.3 Simultaneous Measurements of Oxygen and Fuel . . . . .	19
2.2.3.1 Experimental Setup and Calibration Procedure . . . . .	20
2.2.3.2 Application of Oxygen Measurements . . . . .	20
2.3 Modeling . . . . .	21
2.3.1 Modeling with a Detailed Chemical Mechanism . . . . .	21
2.3.1.1 Kinetic Scheme Validation . . . . .	24
2.3.1.2 Fast and Slow Combustion Modeling . . . . .	26

2.3.1.3	Heat Production and Losses . . . . .	26
2.3.1.4	Radicals and Atoms Rate of Production . . . . .	28
2.3.1.5	Reaction Pathway Diagrams . . . . .	31
2.3.1.6	Explosion Limits . . . . .	35
2.3.1.7	Parametric Study in $\alpha$ , $\phi$ , and $P_0$ . . . . .	37
2.3.2	Modeling with a One-Step Mechanism . . . . .	42
2.4	Theoretical Considerations . . . . .	46
2.4.1	Ignition With Negligible Consumption . . . . .	47
2.4.1.1	Dominant Chemical Energy Release . . . . .	47
2.4.1.2	Effect of Ramp Rate on Induction Time . . . . .	48
2.4.1.3	Critical Heat Transfer . . . . .	50
2.4.1.4	Critical Time For Wall Temperature Ramp . . . . .	51
2.4.2	Ignition With Consumption . . . . .	54
2.4.2.1	Induction Time With Consumption . . . . .	54
2.4.2.2	Thermal Ignition with heat-loss, Consumption, and Wall Temperature Ramp . . . . .	56
2.5	Conclusion . . . . .	61
<b>3</b>	<b>Thermal Ignition and Flame Propagation from a Concentrated Hot Surface</b>	<b>63</b>
3.1	Introduction . . . . .	63
3.2	Experimental Setup . . . . .	64
3.2.1	Composition Uncertainties . . . . .	68
3.2.2	Peak Pressure . . . . .	69
3.2.3	Hot Surface I — High-Temperature Glow Plug (Bosch) . . . . .	71
3.2.4	Hot Surface II — Standard Glow Plug (Autolite 1110) . . . . .	72
3.3	Ignition Temperature . . . . .	73
3.3.1	Hot Surface Ignition Temperature as a Function of Composition . . . . .	74
3.4	Ignition Modeling . . . . .	75
3.4.1	Modeling Background . . . . .	75
3.4.2	Simplified Analytical Approach . . . . .	75
3.4.3	Boundary Layer Modeling Approach . . . . .	78
3.4.3.1	Thermal Ignition Using Tabulated and Detailed Chemistry Modeling . . . . .	90
3.4.4	Hot Surface Ignition Temperature as a Function of Pressure . . . . .	93

3.4.5	Hot Surface Ignition Temperature as a Function of Surface Area . . . . .	94
3.5	Flame Propagation . . . . .	97
3.5.1	Experiments . . . . .	97
3.5.2	Flame Propagation Speed as a Function of Composition . . . . .	99
3.5.3	Computational Modeling of Flame Propagation . . . . .	102
3.5.3.1	Chemistry Tabulation . . . . .	102
3.5.3.2	Reaction Mechanism . . . . .	103
3.5.4	Effect of the Thermal Plume on the Flame Propagation Speed . . . . .	105
3.5.5	Combustion Modes . . . . .	109
3.5.5.1	Single Flames . . . . .	109
3.5.5.2	Multiple Flames . . . . .	110
3.5.5.3	Puffing Flames . . . . .	110
3.5.5.4	Combustion Mode as a Function of Richardson Number . . . . .	111
3.6	Conclusion . . . . .	113
<b>4</b>	<b>Cyclic Flame Propagation in a Fully Premixed Initially Stagnant Mixture</b>	<b>115</b>
4.1	Introduction . . . . .	115
4.2	Experiments . . . . .	116
4.2.1	Experimental Setup and Procedure . . . . .	116
4.2.2	Experimental Observations . . . . .	117
4.2.3	Numerical Simulations . . . . .	118
4.3	Results — Puffing Frequency . . . . .	119
4.3.1	Glow Plug Size and Vessel Size . . . . .	120
4.3.2	Scaling Laws . . . . .	121
4.3.2.1	Cetegen and Ahmed (1993) . . . . .	121
4.3.2.2	Durox et al. (1996) . . . . .	123
4.3.3	Effect of Gravity . . . . .	124
4.3.4	Effect of Flame Speed . . . . .	125
4.3.5	Lean Hexane Puffing Flames . . . . .	127
4.4	Physics of Puffing . . . . .	129
4.4.1	Flow Field Analysis . . . . .	129
4.4.2	Onset of Puffing — Flow Velocity vs. Flame Velocity . . . . .	139
4.5	Conclusions . . . . .	142

<b>5 Conclusions</b>	<b>143</b>
<b>Bibliography</b>	<b>157</b>
<b>A Absorption Measurements for Hydrocarbon Fuel</b>	<b>159</b>
A.1 Direct Absorption Measurements . . . . .	159
A.2 Absorption Cross Sections . . . . .	165
<b>B Second Harmonic Detection of Oxygen with Tunable Diode Lasers</b>	<b>167</b>
B.1 Experimental Setup Addendum . . . . .	170
<b>C Heated Vessel Theory</b>	<b>173</b>
C.1 Governing Equation and Nomenclature . . . . .	173
C.2 Induction Time . . . . .	175
C.2.1 Alternative Derivation . . . . .	176
C.2.2 Frank-Kamenetskii Approximation . . . . .	178
C.2.3 Wall Temperature Ramp Without Chemistry . . . . .	179
C.2.4 Ramp Rate Reduced Induction Time . . . . .	179
C.2.5 Critical Heat-Loss Rate With Constant Wall Temperature . . . . .	181
C.3 Full Nondimensional Equations . . . . .	181
<b>D Collision Limit Calculation for Pre-Exponential</b>	<b>183</b>
<b>E Correlation of Hot Surface Ignition Temperature with Surface Area</b>	<b>185</b>
<b>F Flame Propagation</b>	<b>191</b>
F.1 Introduction . . . . .	191
F.2 Flame Propagation Speed as a Function of Composition . . . . .	192
F.3 Tabular Flame Speed Data . . . . .	195
F.4 Tabular Expansion Ratio Data . . . . .	196
<b>G Thermal Plume Scaling</b>	<b>197</b>
<b>H Refitting Thermodynamic Data</b>	<b>201</b>
<b>I Experimental Data</b>	<b>207</b>
I.1 Heated Vessel Ignition . . . . .	207

I.2 Hot Surface Ignition . . . . .	219
<b>J Ignition Location</b>	<b>227</b>
<b>K Schlieren Sequences</b>	<b>231</b>
<b>L Selected Color Schlieren Images</b>	<b>341</b>
<b>M Hot Surface Temperature and Pressure Traces</b>	<b>347</b>

# List of Figures

1.1	ASTM E 659 auto-ignition temperature apparatus (ASTM, 2005) . . . . .	4
1.2	Ignition as a function of hot surface size (reproduced from Kuchta et al., 1965) . . . . .	5
1.3	Regions of ignition as a function of temperature and pressure for <i>n</i> -hexane (Townend et al., 1934) . . . . .	6
2.1	Schematic of the experimental setup (all dimensions are in cm) . . . . .	15
2.2	Pictures of the heated experimental vessel setup . . . . .	16
2.3	Slow reaction of a fuel-rich ( $\phi = 1.2$ ) <i>n</i> -hexane/air mixture at an initial pressure of 101 kPa heated at 4.25 K per minute . . . . .	17
2.4	Ignition of a fuel-rich ( $\phi = 1.2$ ) <i>n</i> -hexane/air mixture at an initial pressure of 101 kPa heated at 11 K per minute . . . . .	18
2.5	Experimental results as a function of total pressure, temperature ramp rate, and equivalence ratio . . . . .	19
2.6	Schematic of the experimental setup for molecular oxygen measurements . . . . .	21
2.7	Calibration curve, second harmonic peak height as a function of molecular oxygen partial pressure with $\pm \sigma$ uncertainty bars ( $O_2$ only and $O_2$ with 67 kPa $N_2$ dilution) . . . . .	22
2.8	Measurement of the molecular oxygen and fuel concentration during a slow reaction for a <i>n</i> -hexane/air mixture. Conditions: $P_0 = 26.67$ kPa, $\phi = 1.2$ , $\alpha = 11.2$ K/min . . . . .	22
2.9	Comparison of shock tube experimental data to the predictions of the Ramirez model for <i>n</i> -hexane-oxygen-argon mixture . . . . .	25
2.10	Comparison of flow and jet-stirred reactor experimental data to the predictions of the Ramirez model for <i>n</i> -heptane-oxygen-nitrogen mixtures . . . . .	25
2.11	Simulated temperature and pressure profiles for a <i>n</i> -hexane-air mixture for two different heating rates. Conditions: $\phi = 1.2$ (a) $\alpha = 5$ K/min (b) $\alpha = 10$ K/min . . . . .	27
2.12	Simulated species profiles for a <i>n</i> -hexane-air mixture for two different heating rates. Conditions: $\phi = 1.2$ (a) $\alpha = 5$ K/min (b) $\alpha = 10$ K/min . . . . .	27

2.13	Chemical heat production and heat-loss rates for a <i>n</i> -hexane-air mixture for two different heating rates. Conditions: $\Phi = 1.2$ ; $\alpha = 5$ K/min and $\alpha = 10$ K/min (Ignition — Ign, Slow Reaction — SR) . . . . .	28
2.14	Net energy release rate during (a) slow reaction and (b) ignition . . . . .	29
2.15	Rate of production of H atoms and OH radicals for a $\Phi = 1.2$ <i>n</i> -hexane-air mixture and two different heating rates: (a) and (b), $\alpha = 5$ K/min; (c) and (d), $\alpha = 10$ K/min	30
2.16	Carbon reaction pathways during the first phase of a <i>n</i> -hexane-air mixture oxidation for two heating rates. Conditions: $\Phi = 1.2$ ; $\alpha = 5$ and 10 K/min. Black arrows: common pathways. Blue arrows: additional pathways observed during the slow reaction. The first phase extends from 2350 to 2850 s for the slow reaction and from 1220 to 1430 s for the fast reaction. . . . .	33
2.17	Carbon reaction pathways during the second phase of a <i>n</i> -hexane-air mixture oxidation for two heating rates. The second phase extends from 2850 to 3100 s for the slow reaction and from from 1430 to 1495 s for the fast reaction. . . . .	34
2.18	Thermodynamic state trajectories along with the explosion limits (Kane et al., 1937) for a <i>n</i> -hexane-air mixture with different heating rates. Conditions: $\phi = 1.2$ ; $\alpha = 5$ and 10 K/min; (a): temporal evolution (500 s elapsed time between points). (b): <i>n</i> -hexane percentage consumed in the boxed region of (a) . . . . .	36
2.19	Peak overpressure as a function of initial pressure . . . . .	37
2.20	Peak overpressure as a function of heating rate . . . . .	39
2.21	Peak overpressure as a function of equivalence ratio . . . . .	39
2.22	Fast reaction and slow reaction cases as a function of equivalence ratio and heating rate at an initial pressure of one atmosphere . . . . .	40
2.23	Fast reaction and slow reaction cases as a function of equivalence ratio and heating rate at an initial pressure of one atmosphere (fine grid) . . . . .	41
2.24	Transition limits from slow reaction case to ignition cases as function of the initial pressure, equivalence ration, and heating rate . . . . .	41
2.25	Ignition delay time as a function of reciprocal temperature for a stoichiometric hexane-air mixture at atmospheric pressure. The activation energy at low temperatures is estimated by the slope indicated. . . . .	44
2.26	Simulated slow reaction for a heating rate of $\alpha = 5$ K/min using one-step chemistry; (a) reaction progress, (b) temperature . . . . .	45

2.27	Simulated ignition for a heating rate of $\alpha = 10$ K/min using one-step chemistry; (a) reaction progress, (b) temperature . . . . .	45
2.28	Ramp rate reduced induction time . . . . .	50
2.29	Absolute values of heat release and heat-loss components of the energy equation (after Law, 2006) . . . . .	51
2.30	Heat release and heat-loss with a wall temperature ramp . . . . .	53
2.31	Temperature (a) and reaction progress (b) for a slow reaction case and (8 K/min) and an ignition case (10 K/min) . . . . .	57
2.32	Temperature with varying heating rate, $\alpha$ . . . . .	57
2.33	Reaction progress with varying heating rate, $\alpha$ . . . . .	58
2.34	Temperature vs. reaction progress with varying heating rate, $\alpha$ . . . . .	58
2.35	Temperature evolution about the transition point as a function of heating rate . . . .	61
3.1	Diagram of the vessel, flow plug mounting fixture with stagnation surface, field of view (FOV), and glow plug (in red), with dimensions in mm . . . . .	65
3.2	Photograph of the hot surface ignition vessel with an array of thermocouples above the hot surface . . . . .	65
3.3	Schlieren setup schematic . . . . .	66
3.4	Example of color schlieren picture . . . . .	67
3.5	Dark background schlieren visualization of the flame propagation . . . . .	67
3.6	Temperature measurement at the top of the combustion vessel during the ignition of a hexane-air mixture ( $\phi = 1.2$ ) . . . . .	68
3.7	Hot surface experiment plumbing diagram . . . . .	69
3.8	Pressure during the ignition of a hexane-air mixture ( $\phi = 1.2$ ) . . . . .	70
3.9	Peak pressure as a function of equivalence ratios at atmospheric pressure . . . . .	70
3.10	High-temperature glow plug schematic . . . . .	71
3.11	High-temperature glow plug temperature distribution . . . . .	71
3.12	Autolite glow plug schematic . . . . .	72
3.13	Autolite glow plug temperature distribution . . . . .	72
3.14	Temperature of the glow plug during the ignition of a hexane-air mixture ( $\phi = 1.2$ ) .	73
3.15	Hot surface ignition temperature as a function of equivalence ratio at atmospheric pressure for different hot surface sizes . . . . .	74
3.16	Thermal boundary layer along a vertical hot plate . . . . .	79

3.17	Temperature profile in a thermal boundary layer along a vertical hot plate . . . . .	83
3.18	Ignition times for n-heptane and air mixtures computed with the detailed chemical mechanism of Curran et al. (1998) . . . . .	85
3.19	Energy release rate and energy loss rate along a fluid trajectory . . . . .	89
3.20	Trajectories and ignition location along a vertical hot surface . . . . .	89
3.21	Nondimensional temperature profile and velocity profile for a constant and variable density boundary layer along a vertical hot plate (from Cairnie and Harrison, 1982) .	90
3.22	Comparison of ignition locations for different hot surface temperatures . . . . .	92
3.23	Hot surface ignition temperature from tabulated chemistry simulations and experiments	92
3.24	Ignition delay times for n-heptane and air mixtures computed with the detailed chemical mechanism of Curran et al. (1998) . . . . .	93
3.25	Simulated ignition temperatures and ignition times as function of pressure . . . . .	94
3.26	Ignition as a function of hot surface size . . . . .	95
3.27	Flame position grid . . . . .	98
3.28	Representative digitization of the flame location and fitting from shot 33 . . . . .	98
3.29	Spherical flame schematic . . . . .	99
3.30	Flame propagation speed for n-hexane air mixtures as a function of equivalence ratio atmospheric pressure . . . . .	101
3.31	Flame propagation speed at room temperature and atmospheric pressure . . . . .	104
3.32	Dark background schlieren visualization of the flame propagation for a hexane-air mixture (Bosch glow plug, $\phi = 1.2$ ) . . . . .	105
3.33	Simulation results for flame propagation phenomena (Bosch glow plug, $\phi = 1.2$ ) . . .	105
3.34	Laminar burning speed as function of equivalence ratio at different temperatures as calculated using the CaltechMech . . . . .	106
3.35	Comparison between laminar burning speeds calculated using n-heptane-air reaction mechanism and experiments . . . . .	106
3.36	Laminar burning velocity of <i>n</i> -heptane vs. temperature . . . . .	106
3.37	(a) Photograph of the thermocouple array in the vessel used to determine the plume temperature; (b) schlieren image during shot 61 with the thermocouple array in place	107
3.38	(a) Temperature distribution above the glow plug without ignition; (b) temperature distribution above the glow plug . . . . .	108

3.39	Temperature distribution in air above the glow plug comparing simulations and thermocouple measurements . . . . .	108
3.40	Schlieren visualization of a single flame ignited at the glow plug . . . . .	109
3.41	Schlieren visualization of a sequence of two flames ignited at the glow plug . . . . .	110
3.42	Schlieren visualization of puffing behavior . . . . .	111
3.43	Ignition behavior as function of Richardson number for varying initial pressure and equivalence ratio . . . . .	112
4.1	Schlieren images of ignition and subsequent flame propagation in a mixture of hexane in air at atmospheric pressure ( $\phi = 3.0$ ) . . . . .	116
4.2	Direct imaging of CH* molecules through a bandpass filter ( $\lambda_c = 460$ nm with FWHM 40 nm) and a short-pass filter (transmittance > 75% in the range of $\lambda = 430$ –500 nm), $\phi = 3.0$ . . . . .	117
4.3	Transmission curve of the combined filter and CH* spectrum . . . . .	119
4.4	Simulation results (density contours) for flame propagation phenomena at an equivalence ratio of $\phi = 2.5$ . The black line represents the location of the flame front as marked by the iso-contour of the progress variable, $C = 0.15$ . . . . .	120
4.5	Diagrams of pool fire diameter and premixed flame diameter . . . . .	122
4.6	Puffing frequency as a function of gravitational acceleration and pressure . . . . .	124
4.7	Puffing period vs. horizontal flame propagation speed for n-hexane air mixtures from $\phi = 2.15$ –3.0, 7% and 8% hydrogen in air and hexane/hydrogen/air mixtures at atmospheric pressure . . . . .	127
4.8	Flame propagation speeds of hydrogen-air, n-hexane-air, and hydrogen-n-hexane-air mixtures at atmospheric pressure . . . . .	128
4.9	Radial velocity profile at 50 ms . . . . .	130
4.10	Flow field and axial velocity . . . . .	132
4.11	The vorticity production terms along the flame front and resulting vorticity at $t = 50$ ms	133
4.12	Gradients of density, pressure and the resulting baroclinic torque and overall vorticity along the flamefront at $t = 50$ ms associated with the incipient puff . . . . .	135
4.13	Detailed vorticity distribution . . . . .	135
4.14	Density as a function of radial location at different locations in the flame . . . . .	136
4.15	Vorticity as a function of radial location at different locations in the flame . . . . .	136
4.16	Axial velocity as a function of radial location at different locations in the flame . . . . .	137

4.17	Radial velocity as a function of radial location at different locations in the flame . . .	137
4.18	Flame propagation speed along the the flame front as a function of time . . . . .	140
4.19	Inflow velocity along the the flame front as a function of time. Positive velocities mean flow going from unburned to burned side. . . . .	141
4.20	Inflow velocity and flame propagation velocity along the the flame front as a function of time showing the 10 Hz frequency observed in experiments and simulations . . . . .	141
A.1	Beer's law diagram . . . . .	160
A.2	Fuel detection experimental setup . . . . .	162
A.3	Judson detector . . . . .	162
A.4	Detector circuit . . . . .	163
A.5	Raw fuel data from shot 19 . . . . .	164
B.1	Raw oxygen 2f data from shot 19 . . . . .	171
E.1	Ignition as a function of hot surface size. . . . .	189
F.1	Laminar burning velocity at room temperature and atmospheric pressure . . . . .	192
F.2	Laminar burning velocity at 353 K and atmospheric pressure . . . . .	193
F.3	Experimental flame propagation speed . . . . .	193
F.4	Flame propagation speed at room temperature and atmospheric pressure . . . . .	194
G.1	Plume temperature scaling and thermocouple measurements . . . . .	199
H.1	Original thermodynamic data - $c_p/R$ . . . . .	201
H.2	New thermodynamic data - $c_p/R$ . . . . .	203
I.1	Experimental data from shot 13 . . . . .	210
I.2	Experimental data from shot 14 . . . . .	210
I.3	Experimental data from shot 16 . . . . .	211
I.4	Experimental data from shot 17 . . . . .	211
I.5	Experimental data from shot 19 . . . . .	212
I.6	Experimental data during the ignition event from shot 19 . . . . .	212
I.7	Experimental data from shot 20 . . . . .	213
I.8	Experimental data during the ignition event from shot 20 . . . . .	213
I.9	Experimental data from shot 21 . . . . .	214

I.10	Experimental data from shot 22 . . . . .	214
I.11	Experimental data from shot 23 . . . . .	215
I.12	Experimental data during the ignition event from shot 23 . . . . .	215
I.13	Experimental data from shot 24 . . . . .	216
I.14	Experimental data from shot 25 . . . . .	216
I.15	Experimental data from shot 26 . . . . .	217
I.16	Experimental data from shot 37 . . . . .	218
I.17	Experimental data from shot 40 . . . . .	218
I.18	Experimental data during the ignition event from shot 40 . . . . .	218
I.19	Picture of the hot surface ignition vessel experimental setup . . . . .	219
J.1	Ignition locations observed in schlieren videos . . . . .	227
J.2	Ignition locations observed in schlieren videos (continued) . . . . .	228
J.3	Ignition locations observed in schlieren videos (continued) . . . . .	229
K.1	Shot 6 . . . . .	231
K.2	Shot 7 . . . . .	232
K.3	Shot 8 . . . . .	233
K.4	Shot 9 . . . . .	234
K.5	Shot 10 . . . . .	235
K.6	Shot 15 . . . . .	236
K.7	Shot 17 . . . . .	237
K.8	Shot 17 montage . . . . .	238
K.9	Shot 20 . . . . .	239
K.10	Shot 21 . . . . .	240
K.11	Shot 22 . . . . .	241
K.12	Shot 24 . . . . .	242
K.13	Shot 25 . . . . .	243
K.14	Shot 26 . . . . .	244
K.15	Shot 27 . . . . .	245
K.16	Shot 28 . . . . .	246
K.17	Shot 29 . . . . .	247
K.18	Shot 30 . . . . .	248

K.19	Shot 31	249
K.20	Shot 32	250
K.21	Shot 33	251
K.22	Shot 34	252
K.23	Shot 36	253
K.24	Shot 37	254
K.25	Shot 38	255
K.26	Shot 40	256
K.27	Shot 41	257
K.28	Shot 41 montage	258
K.29	Shot 42	259
K.30	Shot 42 montage	260
K.31	Shot 43	261
K.32	Shot 44	262
K.33	Shot 44 montage	263
K.34	Shot 45	264
K.35	Shot 45 montage	265
K.36	Shot 46	266
K.37	Shot 47	267
K.38	Shot 48	268
K.39	Shot 48 montage	269
K.40	Shot 49	270
K.41	Shot 49 montage	271
K.42	Shot 50	272
K.43	Shot 50 montage	273
K.44	Shot 51	274
K.45	Shot 52	275
K.46	Shot 54	276
K.47	Shot 54 montage	277
K.48	Shot 55	278
K.49	Shot 57	279
K.50	Shot 58	280

K.51	Shot 58 montage . . . . .	281
K.52	Shot 60 . . . . .	282
K.53	Shot 60 montage . . . . .	283
K.54	Shot 61 . . . . .	284
K.55	Shot 64 . . . . .	285
K.56	Shot 65 . . . . .	286
K.57	Shot 66 . . . . .	287
K.58	Shot 68 . . . . .	288
K.59	Shot 69 . . . . .	289
K.60	Shot 69 montage . . . . .	290
K.61	Shot 70 . . . . .	291
K.62	Shot 73 . . . . .	292
K.63	Shot 76 . . . . .	293
K.64	Shot 76 montage . . . . .	294
K.65	Shot 77 . . . . .	295
K.66	Shot 77 montage . . . . .	296
K.67	Shot 80 . . . . .	297
K.68	Shot 80 montage . . . . .	298
K.69	Shot 81 . . . . .	299
K.70	Shot 81 montage . . . . .	300
K.71	Shot 85 (Note the drop of molten copper visible below the hot surface holder in the last two frames) . . . . .	301
K.72	Shot 86 . . . . .	302
K.73	Shot 86 montage . . . . .	303
K.74	Shot 87 . . . . .	304
K.75	Shot 87 montage . . . . .	305
K.76	Shot 90 . . . . .	306
K.77	Shot 90 montage . . . . .	307
K.78	Shot 91 . . . . .	308
K.79	Shot 91 montage . . . . .	309
K.80	Shot 92 . . . . .	310
K.81	Shot 93 . . . . .	311

K.82	Shot 94 . . . . .	312
K.83	Shot 97 . . . . .	313
K.84	Shot 98 . . . . .	314
K.85	Shot 98 montage . . . . .	315
K.86	Shot 100 . . . . .	316
K.87	Shot 100 montage . . . . .	317
K.88	Shot 101 . . . . .	318
K.89	Shot 101 montage . . . . .	319
K.90	Shot 102 . . . . .	320
K.91	Shot 103 . . . . .	321
K.92	Shot 103 montage . . . . .	322
K.93	Shot 104 . . . . .	323
K.94	Shot 104 montage . . . . .	324
K.95	Shot 110 . . . . .	325
K.96	Shot 110 montage . . . . .	326
K.97	Shot 112 . . . . .	327
K.98	Shot 112 montage . . . . .	328
K.99	Shot 115 . . . . .	329
K.100	Shot 116 . . . . .	330
K.101	Shot 117 . . . . .	331
K.102	Shot 118 . . . . .	332
K.103	Shot 118 montage . . . . .	333
K.104	Shot 119 . . . . .	334
K.105	Shot 119 montage . . . . .	335
K.106	Shot 121 . . . . .	336
K.107	Shot 122 . . . . .	337
K.108	Shot 123 . . . . .	338
K.109	Shot 123 montage . . . . .	339
L.1	Color schlieren images from shot 28 . . . . .	342
L.2	Color schlieren images from shot 30 . . . . .	342
L.3	Color schlieren images from shot 33 . . . . .	342
L.4	Color schlieren images from shot 34 . . . . .	343

L.5	Color schlieren images from shot 36 . . . . .	343
L.6	Color schlieren images from shot 41 . . . . .	343
L.7	Color schlieren images from shot 42 . . . . .	344
L.8	Color schlieren images from shot 45 . . . . .	345
M.1	Experimental data from shot 7 . . . . .	348
M.2	Experimental data from shot 8 . . . . .	348
M.3	Experimental data from shot 9 . . . . .	349
M.4	Experimental data from shot 10 . . . . .	349
M.5	Experimental data from shot 11 . . . . .	350
M.6	Experimental data from shot 12 . . . . .	350
M.7	Experimental data from shot 15 . . . . .	351
M.8	Experimental data from shot 17 . . . . .	351
M.9	Experimental data from shot 20 . . . . .	352
M.10	Experimental data from shot 21 . . . . .	352
M.11	Experimental data from shot 22 . . . . .	353
M.12	Experimental data from shot 23 . . . . .	353
M.13	Experimental data from shot 24 . . . . .	354
M.14	Experimental data from shot 25 . . . . .	354
M.15	Experimental data from shot 26 . . . . .	355
M.16	Experimental data from shot 28 . . . . .	355
M.17	Experimental data from shot 28 . . . . .	356
M.18	Experimental data from shot 29 . . . . .	356
M.19	Experimental data from shot 30 . . . . .	357
M.20	Experimental data from shot 31 . . . . .	357
M.21	Experimental data from shot 32 . . . . .	358
M.22	Experimental data from shot 33 . . . . .	358
M.23	Experimental data from shot 34 . . . . .	359
M.24	Experimental data from shot 36 . . . . .	359
M.25	Experimental data from shot 37 . . . . .	360
M.26	Experimental data from shot 38 . . . . .	360
M.27	Experimental data from shot 40 . . . . .	361
M.28	Experimental data from shot 41 . . . . .	361

M.29	Experimental data from shot 42	362
M.30	Experimental data from shot 43	362
M.31	Experimental data from shot 44	363
M.32	Experimental data from shot 45	363
M.33	Experimental data from shot 46	364
M.34	Experimental data from shot 47	364
M.35	Experimental data from shot 49	365
M.36	Experimental data from shot 50	365
M.37	Experimental data from shot 51	366
M.38	Experimental data from shot 54	366
M.39	Experimental data from shot 55	367
M.40	Experimental data from shot 57	367
M.41	Experimental data from shot 58	368
M.42	Experimental data from shot 61	368
M.43	Experimental data from shot 64	369
M.44	Experimental data from shot 65	369
M.45	Experimental data from shot 68	370
M.46	Experimental data from shot 69	370
M.47	Experimental data from shot 70	371
M.48	Experimental data from shot 85	371
M.49	Experimental data from shot 86	372
M.50	Experimental data from shot 87	372
M.51	Experimental data from shot 90	373
M.52	Experimental data from shot 91	373
M.53	Experimental data from shot 92	374
M.54	Experimental data from shot 93	374
M.55	Experimental data from shot 94	375
M.56	Experimental data from shot 95	375
M.57	Experimental data from shot 96	376
M.58	Experimental data from shot 97	376
M.59	Experimental data from shot 98	377
M.60	Experimental data from shot 100	377

M.61	Experimental data from shot 101 . . . . .	378
M.62	Experimental data from shot 102 . . . . .	378
M.63	Experimental data from shot 103 . . . . .	379
M.64	Experimental data from shot 104 . . . . .	379
M.65	Experimental data from shot 115 . . . . .	380
M.66	Experimental data from shot 116 . . . . .	380
M.67	Experimental data from shot 117 . . . . .	381
M.68	Experimental data from shot 118 . . . . .	381
M.69	Experimental data from shot 119 . . . . .	382
M.70	Experimental data from shot 121 . . . . .	382
M.71	Experimental data from shot 122 . . . . .	383
M.72	Experimental data from shot 123 . . . . .	383

# List of Tables

1.1	Selected minimum auto-ignition temperatures (AIT) at one atmosphere from Kuchta (1985) and CRC (1983) . . . . .	7
2.1	Nomenclature . . . . .	42
2.2	Parameters used in modeling of hexane-air auto-ignition . . . . .	44
3.1	Parameters used in modeling of hexane-air hot surface ignition . . . . .	86
4.1	Puffing behavior for fuel-rich hexane air mixture ( $\phi = 3.0$ ) . . . . .	121
A.1	Uncertainty in fuel concentration measurements . . . . .	161
A.2	Absorption cross sections . . . . .	165
C.1	Nomenclature . . . . .	173
C.2	Additional nomenclature . . . . .	174
F.1	Laminar burning velocity ( $S_l$ ) for $n$ -hexane and $n$ -heptane at atmospheric pressure ( $P_0 = 101$ kPa) . . . . .	195
F.2	Expansion ratio for $n$ -hexane and $n$ -heptane at atmospheric pressure ( $P_0 = 101$ kPa), room temperature ( $T_u = 300$ K) computed using the thermodynamic data from the Ramirez mechanism (Ramirez et al., 2011) . . . . .	196
I.1	Heated vessel experiments . . . . .	209
I.2	Hot surface experiments ( $n$ -hexane, Bosch glow plug) . . . . .	220
I.3	Hot surface experiments ( $n$ -hexane, Bosch glow plug, continued) . . . . .	221
I.4	Hot surface experiments ( $n$ -hexane, Autolite glow plug) . . . . .	222
I.5	Hot surface experiments ( $n$ -heptane, Autolite glow plug) . . . . .	223
I.6	Spark ignition experiments ( $n$ -hexane) . . . . .	223
I.7	Hot surface experiments ( $n$ -hexane, Autolite glow plug, large vessel) . . . . .	224

I.8	Hot surface experiments ( <i>n</i> -hexane, varying hot surface, 2 liter vessel) . . . . .	224
I.9	Hot surface experiments (hydrogen, Autolite glow plug, small vessel) . . . . .	225
I.10	Hot surface experiments (hydrogen-hexane-air mixtures, Autolite glow plug, small vessel)	225

This page intentionally left blank.

# Chapter 1

## Introduction

### 1.1 Motivation

Accidental ignition of flammable gases is a critical safety concern in many industrial applications. Particularly in the aviation industry, the main areas of concern on an aircraft are the fuel tank and adjoining regions, where spilled fuel has a high likelihood of creating a flammable mixture. To this end, a fundamental understanding of the ignition phenomenon is necessary in order to develop more accurate test methods and standards as a means of designing safer air vehicles.

Following the TWA 800 accident on July 17, 1996, the National Transportation Safety Board (NTSB) investigated the fuel tank flammability and fuel tank ignition sources (NTSB, 2000). The results of investigation led the NTSB to recommend that the FAA find a means to eliminate flammable mixtures in the fuel tanks. In 2008, the FAA created a requirement to install an inerting system to eliminate flammability, particularly for heated center fuel tanks by reducing the oxygen content below 12%. As part of the NTSB investigation, several research projects were carried out at the Explosion Dynamics Laboratory at California Institute of Technology including: “Flash Point and Chemical Composition of Aviation Kerosene (Jet A)” (Shepherd et al., 1999), Spark Ignition Energy Measurements in Jet A (Shepherd et al., 1997). While not directly addressed in the final FAA rule-making, the reduction or elimination of possible ignition sources is an essential part of engineering design practices for aircraft and industries with flammability hazards. In this regard, Shepherd et al. (1997) investigated the required ignition energy for Jet A, while Bane et al. (2011) showed that kerosene mixtures have comparable minimum ignition energy to the lean hydrogen mixtures used for certification. The lean hydrogen mixtures were assumed to have lower ignition energies and thus using them as test mixtures would have an inherent safety margin. In light of the findings by Bane et al. (2011) we were motivated to investigate the test standards currently in use for thermal

ignition, i.e., in heated vessel or by hot surfaces. There are of course other potential ignition sources such as open flames, electrical streamer discharges, hot and burning particles, but these were not the focus of this study.

For safety aspects, several different temperatures are important for the characterization of a particular fuel. Colwell and Reza (2005) describe how the temperature required for ignition increases given the situation. For example, the flash point is the temperature above which a pool of liquid fuel has sufficient vapor pressure to be ignited by a pilot flame (ASTM, 2010). The flash point of Jet A lies in the range of 43–66 °C (Colwell and Reza, 2005, CRC, 1983, NFPA 325, 1994). If we were to take the flash point as a general upper bound for any design temperature, we would be unable to boil water for coffee or tea on an aircraft. This, of course, is not the case since no open flame is present near the fuel tank, by design.

For ignition from hot elements, the particular quantity of interest is the temperature that leads to ignition of a flammable atmosphere without a flame present. A measure of this temperature is defined as the auto-ignition temperature. The auto-ignition temperature standard test is to inject a fuel into a heated vessel and determine by visual inspection if ignition has occurred within 10 minutes (ASTM, 2005). For many applications, the auto-ignition temperature determined from this standard test is what is then used to define limiting (highest) temperature of hot surfaces in region where flammable vapor may be present. However, this test has many limitations, which are explored in the following chapters. The flame propagation resulting from an ignition of a premixed fuel-air mixture determines the pressure rise and thus potential structural damage resulting from an accidental ignition, and must also be considered. The ignition process is a complicated interaction of chemical heat release, encompassing the competition between chain branching and terminating reactions, heat transfer into and out of the system, and fluid mechanics. To mitigate the risk of accidental explosions in industrial facilities and on aircraft in the aviation industry, the mechanisms and parameters leading to ignition must be investigated. The ultimate goal is to use our better understanding of the thermal ignition process and auto-ignition tests to further improve the safety of aviation and other industrial systems operating with flammable mixtures.

## 1.2 Background

Seminal work in the area of ignition by hot surfaces was done by Davy (1817) while investigating explosions in coal mines (Babrauskas, 2003). Davy describes a common way of lighting the mines as:

“a steel wheel, which, being made to revolve in contact with flint, affords a succession of sparks: but this apparatus always requires a person to work it; and, though much less liable to explode the fire-damp than a common candle, yet it is said to be not entirely free from danger.”

In his experiments, Davy was unable to ignite a combustible coal gas (firedamp) mixture with a hot iron rod, unless the iron rod itself is burning. The first explanation of this effect (Babrauskas, 2003) was given by Mallard and Le Chatelier in 1880. They concluded that a sufficiently long time is necessary for the gas to stay in contact with the hot surface in order for the mixture to ignite.

Thornton (1919) was among the first to perform experiments on the current required to ignite various gaseous mixtures by electrical wire, with particular focus on the hazard that arises from broken light bulbs in coal mines. In this work, measurements were performed at elevated pressures using water to compress the gas, and it was concluded that ignition by hot wires is independent of pressure, but changes with wire diameter. These experiments, however, are incomparable to the atmospheric tests since the absorption into the water and water vapor content are not accounted for.

In 1927, Coward and Guest investigated the ignition of natural gas and air mixtures by heated nickel bars of varying size, composition, hot surface material, and flow velocity above the hot surface. The work concluded that the ignition temperature depends on the mixture composition, but an explanation was not provided. Coward and Guest observed that wider heated bars reduce the temperature required for ignition, and that flow over hot surface, created by a fan, could either decrease or increase the ignition temperature depending on the speed.

Scott et al. (1948) used an early version of the auto-ignition test apparatus, which would later become the ASTM E 659 test shown in Figure 1.1. Experimental auto-ignition temperatures are given for a multitude of compounds as part of the experiments at the Bureau of Mines in Pittsburgh, PA.

The Bureau of Mines continued their work, which was published in part in Zabetakis et al. (1954) and Kuchta et al. (1965), performing a wide range of experiments on auto-ignition and hot surfaces using a variety of fuels. In these investigations, experiments were conducted to test the effect

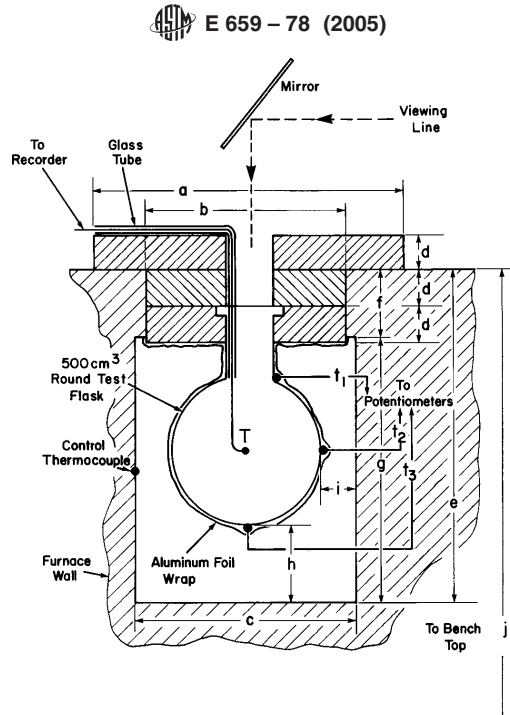


Figure 1.1: ASTM E 659 auto-ignition temperature apparatus (reprinted, with permission, from ASTM (2005), copyright ASTM International)

of surface area and volume on auto-ignition in quiescent mixtures, with the work on hot surfaces performed in a slow flowing reactor. The results of these efforts included a scaling relationship for the ignition temperature as a function of the natural logarithm of the (hot) surface area as shown in Figure 1.2. However, the effects of the surface geometry or orientation are not considered, and consequently the scaling laws extrapolated from theory developed by Semenov (1940) only hold for a limited range of hot surface areas.

The graph reproduced in Figure 1.2 is also found in Babrauskas (2003) without the data points. While the trends developed by Semenov (1940) are supported by this data, the broad application of this work should be taken very cautiously as the control over composition and flow velocity are very limited.

We separate the investigation of thermal ignition into the goal of finding the lowest possible temperature at which a gaseous mixture will ignite, i.e., auto-ignition, and the required temperature for less favorable geometries such as isolated hot surfaces.

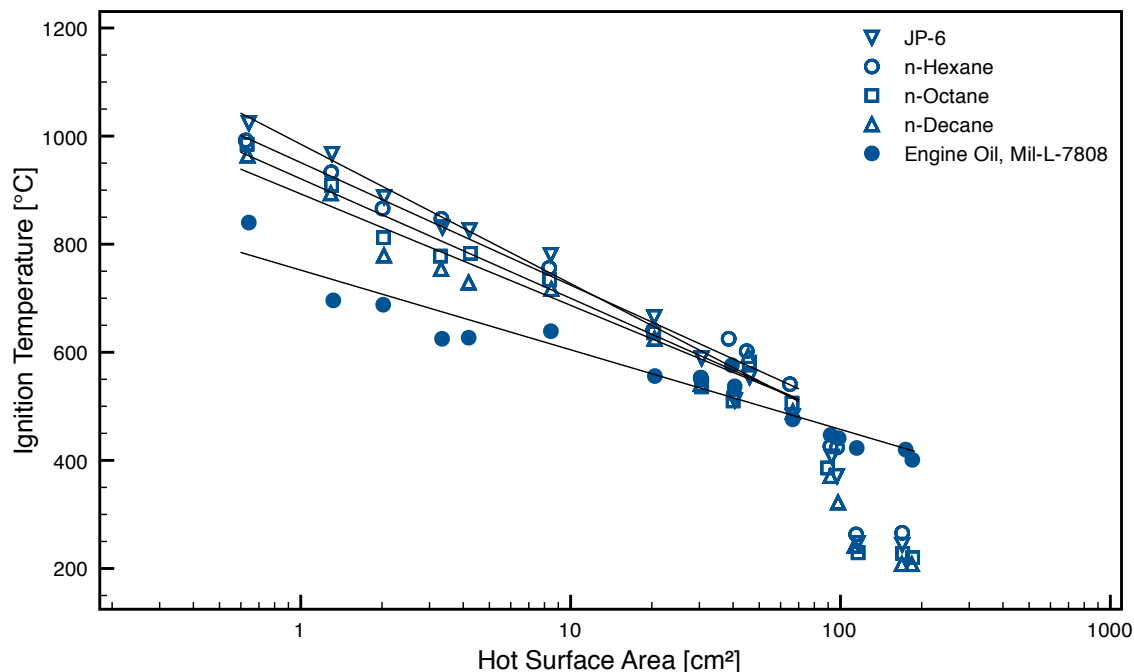


Figure 1.2: Ignition as a function of hot surface size (reproduced from Kuchta et al., 1965)

### 1.2.1 Thermal Ignition in a Heated Vessel — Auto-Ignition

Ignition is the process of initializing an exothermic chemical reaction that can lead to a propagating flame or detonation. Ignition can occur through the generation of highly reactive species (radicals), whose production rate is in competition with their destruction rate, as well as the competition of chemical heat release and heat loss to walls, which determines the mixture temperature and thus the reaction rates. In general, combustion of hydrocarbon fuels is separated into slow reaction, cool flames, and ignition regimes based on pressure and temperature (Glassman, 2008, Pilling, 1997).

Slow reactions occur when fuel is in contact with an oxidizer at temperatures below the ignition temperature (Babrauskas, 2003). The fuel and oxidizer react, but do so without a rapid increase in pressure, and the heat released by the oxidation is lost to the environment. Since the reaction rate is a strong function of temperature, these reactions will not take place at a temperature far below the ignition temperature (Babrauskas, 2003).

Cool flames occur at temperatures higher than slow reaction and below the ignition temperatures (Babrauskas, 2003). This lower temperature leads the reaction down a different path, creating peroxides as reaction products, which are only partially oxidized and thus release less energy than if the reaction had gone to completion (e.g.,  $\text{CO}_2$  and  $\text{H}_2\text{O}$  for hydrocarbon oxygen reac-

tions) (Babrauskas, 2003). The resulting flames have a pale blue color, and can exhibit oscillatory behavior (Yang and Gray, 1969). Townend et al. (1934) were the first to map at what temperatures and pressures ignition and cool flames of hexane air mixtures occur.

From a chemical reaction perspective, ignition is characterized by a “rate of chain carrier generation exceeding the chain termination reaction” - or in other words, a runaway reaction (Glassman, 2008). In this case, the reaction releases energy and thus speeds up the reaction rate if that energy cannot be lost to environment at a sufficiently fast rate. The reaction then leads to a pressure and temperature rise until the reactants are consumed.

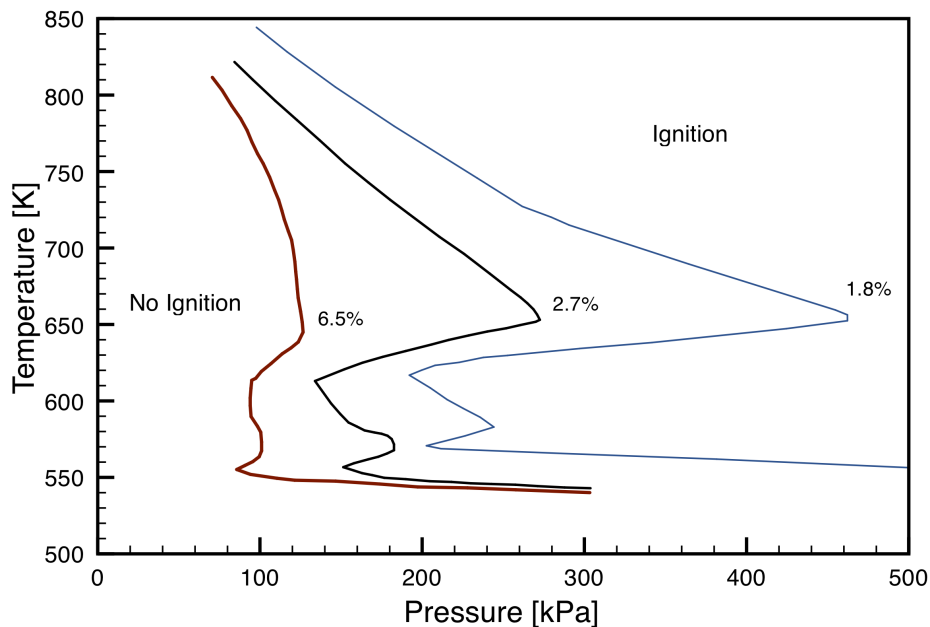


Figure 1.3: Regions of ignition as a function of temperature and pressure for *n*-hexane for several molar concentrations of *n*-hexane in air (Townend et al., 1934) (Figure adapted from Babrauskas, 2003)

A classical view of how ignition, nonignition and cool flames are separated as function of temperature and pressure is given for *n*-hexane as shown in Figure 1.3 (Townend et al., 1934). At low temperature and low pressure some radical species may be formed. Due to the low pressure, the diffusivity is high and they recombine into stable species at wall, which means that testing vessels of different material can have different explosion limits (Warnatz et al., 2006).

The auto-ignition temperature is not a universal quantity and depends on the substance and molecular structure of the fuel as well as the oxidizer and whether or not any diluent are present, e.g., the nitrogen in air. For this investigation, we are interested in fuels like hexane that have comparable auto-ignition temperatures to aviation kerosene (see Table 1.1). The combustion characteristics

and path of pure substances are far more easy to characterize than those of complex hydrocarbon fuels such as Jet A, which consists of many different species of paraffins, iso-paraffins, aromatics, naphthenes, and olefins (Shepherd et al., 1999).

Table 1.1: Selected minimum auto-ignition temperatures (AIT) at one atmosphere from Kuchta (1985) and CRC (1983)

Fuel	AIT [ $^{\circ}$ C]	
	in air	in oxygen
Hydrogen	520	$\sim$ 400
Methane	630	500
Propane	450	N/A
<i>n</i> -Hexane	225	220
Gasoline (100/130)	440	315
Kerosene	230	215
Turbine Fuel	238	N/A

While the ASTM E659 is a standard test for the auto-ignition temperature, only the minimum temperature for ignition at atmospheric pressure is investigated (ASTM, 2005, Colwell and Reza, 2005, Pilling, 1997). The specific mixture composition is not controlled because liquid test fuel is injected directly into an open heated vessel. The contents are not actively mixed, and it is presumed that “a considerable range of composition exist within pockets of gas in the vessel as evaporation of liquid fuel, or mixing of the injected gaseous fuel, occurs” (Pilling, 1997).

In prior laboratory research, the combustion products have either been condensed and the liquid analyzed later (Bailey and Norrish, 1952), or a gas chromatograph was used to analyze a small sample at a maximum frequency of about 0.1 Hz (Wilk et al., 1986). Additional work was done in rapid compression machines at higher temperatures, 600–800 K (Griffiths et al., 1993), and gas sampling techniques (Ribaucour et al., 1992, Vanhove et al., 2006). While pressure transients are easily captured in these experiments, fast and accurate fuel concentration measurements requiring optical techniques have never previously been applied to the auto-ignition phenomenon.

The present work includes tests conducted using hexane as a surrogate for kerosene, with the experimental setup addressing problem of the control over gas composition, allowing for testing at varying pressures, and precise control over the heating rate, which has been identified as an important factor (Mason and Wheeler, 1922). Additionally, the current study allows for continuous measurements of the fuel concentration.

### 1.2.2 Thermal Ignition from a Concentrated Hot Surface

Isolated hot surfaces surrounded by a flammable mixture such as a pipe carrying hot gas in a flammable leakage zone in an aircraft or the overheating of a failing device, are potential ignition sources. For design purposes, it is important to understand the dependence of the ignition temperature on hot surface size and geometry since limiting space restrictions may lead to unfeasible design solutions. While, standardized tests exist to evaluate various properties of fuels, including the ASTM E659 (ASTM, 2005) for auto-ignition temperature of fuels, and the ASTM D56 (ASTM, 2010) for flash point, no standard test exists for hot surface ignition (Smyth and Bryner, 1997).

As mentioned before, Coward and Guest (1927) investigated hot surface ignition of natural gas-air mixture by various heated metal surfaces, but the control over the flow velocity at the hot surface and visual observations were limited. Platinum surfaces were found to be catalytic, but the ignition temperatures were higher than those of noncatalytic nickel. Kuchta et al. (1965) extended the work at the Bureau of Mines, varying the size and geometry of the hot surfaces, but with limited control over the composition and flow over the hot surface. The hot surface of interest is heated to a given temperature inside a flow reactor and then a mixture of fuel and air is passed over it at a specified flow rate. However, the exact mixture composition is unknown and the flow velocity at the hot surface can only be roughly estimated based on the overall flow rate and vessel size.

Gray (1970) analytically investigated the effect of surface area to volume ratio. The work follows the work of Kuchta et al. (1965) and White (1967) who concluded from experimental data that increasing the surface area in a fuel tank, e.g., by inserting metal honeycomb, increases the safety. Gray pointed to the negative temperature coefficient behavior of larger hydrocarbon as an alternate source for the behavior.

Ono et al. (1976) studied the ignition of stoichiometric mixtures of methane, propane, ethyl-alcohol, and diethylether in air by a vertical hot plate inside a combustion vessel. Measurements of the flow velocity were performed by particle image velocimetry. The choice of geometry is quite useful in comparisons with simulations and analytical models for flow along a heated vertical plate (Tritton, 1988). The temperature of the hot surface is initially kept at a temperature just below the ignition temperature and then raised to initiate ignition. As mentioned earlier, slow reactions can take place at temperatures just below the ignition temperature and change the composition of the mixture.

Laurendeau (1982) performed a wide literature review of available hot surface ignition data for various hydrocarbon fuels, particularly methane. The data collected was used to derive a simple correlation relating the ignition temperature to various parameters. Also taken into account in

the model is the flow outside the hot surface, such as stagnant, free, and forced convection. The value of this model is to give general trends of the ignition temperature, but does not provide accurate numerical values. Laurendeau points out that detailed information about the experiments and application are necessary to make accurate comparisons, including the surface size, orientation, geometry, mixture composition, and temperature history leading to ignition.

Kumar (1989) focused his experiments on hydrogen-oxygen-diluent mixtures. The combustion of hydrogen differs from that of hydrocarbon fuel. In addition, its high diffusivity will change the hot surface ignition characteristics relative to hydrocarbon fuels, which must be kept in mind when comparing the results of ignition experiments and simulations. It is still very relevant for many applications including loss-of-cooling events in nuclear power plant like Fukushima–Daiichi on March 11, 2011.

Kumar also developed a model of solving the transport and energy conservation equation using an explicit scheme, that requires very small time steps down to 1 ns for accurate solutions. The equations describe the ignition from a hot surface in one dimensional unsteady condition with the gas at temperature below the hot surface temperature and the chemistry uses a reduced mechanism for hydrogen-oxygen-diluent combustion. In the experiments and simulations, the effects of pressure, mixture concentration, diluent, and initial gas temperature were investigated with relatively good agreement for most parameters.

In an effort to create a standardized test for hot surface ignition, Smyth and Bryner (1997) at the National Institute of Standards and Technology (NIST) performed a large number of experiments testing the temperature required for ignition of a gas mixture flowing over a heated metal foil. In this work, the foil was placed at  $45^\circ$  for a constant residence time of 150 ms, and a wide variety of fuels and hot surface materials were examined. From the results given in their study, the temperature are higher than even those of Kuchta et al. (1965) at comparable surface size, which would indicate that the residence time was too short to activate any low temperature chemistry. Additionally, the geometry chosen for the experiment is very difficult to reproduce computationally (Shepherd, 2012).

Babrauskas (2003) points out that hot surface ignition can be investigated in a similar manner to the auto-ignition tests, where no uniform heating eliminates convection. For hot surfaces, this could be achieved by placing the hot surface at the top of the vessel and thus stably stratifying the mixture, however, no such experiments have been performed.

### 1.2.3 Hot Surface Ignition of Liquid Fuels

A special type of hot surface ignition is ignition of liquid fuel droplet by hot surfaces. This process is significantly more complex due to the breakup of droplet, evaporation of the fuel and mixing with the air necessary to create a flammable mixture. However, the connection to the work presented here is clear and thus worth mentioning. In 2005, Colwell and Reza performed a large number of tests using droplets of fuel impinging a hot surface and evaluating the ignition probability as a function of temperature. While the work included a thorough review of thermal ignition testing on available data, an extrapolation of their results to the fundamental physical and chemical processes leading to hot surface ignition is difficult. The complexity of the experiments performed is too great to use analytical models or even perform simulations and a statistical approach is taken to characterize the likelihood of ignition as a function of temperature. A thorough literature review of ignition of liquid droplets was done by Bennett (2001).

In this study, we explore the conditions leading to ignition and compare these to high quality computational results. Our goal is to develop sufficiently realistic and detailed models so that these ignition thresholds and ignition transients can be accurately predicted.

### 1.2.4 Cyclic Flame Propagation in Premixed Combustion

The process of thermal ignition of a flammable mixture by a hot-surface and the subsequent flame propagation is important to the fundamental understanding of combustion, as well as industrial safety applications. Flame instabilities are of particular interest since they can affect the flame propagation speed and increasing the flame surface area and accelerating the flame speed. This chapter focuses on a global flame instability, i.e., a flickering or puffing flame, rather than small scale instabilities at the flame front.

Flames propagating with a flickering or puffing behavior with frequencies around 10 Hz have been discussed since the First International Symposium on Combustion in September 1928 (Chamberlin and Rose, 1948). Chamberlin and Rose were among the first to make quantitative measurements of the oscillation frequencies observed in Bunsen burners. For a range of gases (e.g., natural gas, hydrogen, carbon monoxide, butane, and ethane), the rate of flame oscillations was observed to be “on the order of 10 per second”. The oscillations were quantified by tracking the tip location of the flame. Chamberlin and Rose observed that frequency changed with the size of the injection nozzle, and the origin of the flicker was attributed to an alternating rate of diffusion of oxygen into the flame

The oscillation of non-premixed gaseous flames have since then been investigated experimentally by Kimura (1965), Toong et al. (1965), Durao and Whitelaw (1974), Grant and Jones (1975), Strawa and Cantwell (1989) and Durox et al. (1996).

Kimura (1965) investigated propane jet flames, which exhibited periodic oscillations (10–15 Hz) above a critical injection velocity. Premixing the propane with air suppressed these oscillations. After investigating the temperature and velocity profile, he concludes that the oscillations are caused by the instability of the laminar jet flow.

Toong et al. (1965) observed these instabilities for flames created by burning liquid fuel at the end of a probe in air to simulate droplet combustion. They postulate that “it is quite likely that the onset of the self-sustained flame oscillations is due to the amplification of the Tollmien-Schlichting waves, in the region where the Reynolds Number is greater than the critical value.” However, Grant and Jones (1975) argue that based on their experiments and those of Durao and Whitelaw (1974), linear stability theory is insufficient in explaining how the frequency is invariant over a large range of parameters.

The jet injection velocity was substantially reduced in the experiments conducted by Durox et al. (1996). In fact, in their theoretical analysis the injection velocity is assumed to be negligible and the flame instability is attributed to a shear layer created by the buoyancy induced velocity on the flow behind the flame front. In their study, the effect of pressure and gravitational acceleration were tested by performing the experiment on parabolic flights that created microgravity as well as maximum accelerations of 1.8 *g*.

Buckmaster and Peters (1988) have carried a theoretical analysis of the oscillations associated with a infinite candle. Similar oscillations have also been observed in fires above pools of liquid fuels (Cetegen and Ahmed, 1993) and in room fires (Zukoski, 1986).

These oscillations are not limited to non-premixed flames, but also occur in premixed flames as shown by Durox et al. (1990), Cheng et al. (1999), Shepherd et al. (2005), Guahk et al. (2009), and Tanoue et al. (2010). In these studies, the frequency of the instability is again on the order of 10 Hz. In all of these previous experiments of premixed flames, the gaseous mixture was injected into the burner at a specific injection velocity.

Durox et al. (1990) also performed experiments on parabolic flights of premixed flames to study the effect of varying gravitational acceleration. Additional data is given for the variation of the oscillation frequency as a function of injection velocity (1.45–2.4 m/s), pressure, and equivalence ratio.

Cheng et al. (1999) studied the effects of buoyancy on premixed “V-flames” by considering both gravitation acceleration in the direction of injection and opposed to it. The results were considered as a function of Richardson number, the ratio of inertia to buoyancy force, but “findings point to the need to include both upstream and downstream contributions in theoretical analysis of flame turbulence interactions.”

Guahk et al. (2009) investigated the oscillations of conical flames and inverted conical flames. They describe the oscillations as a flame-intrinsic Kelvin-Helmholtz instability.

A combined experimental and numerical approach was taken by Shepherd et al. (2005), who injected a methane-air mixture at 0.73 m/s. The analysis showed that the “flame tip oscillation is caused by a competition between the pressure fields associated with the predominantly radial motion of the burnt gases near the flame front and the rotating vortex motion.”

Tanoue et al. (2010) measured the temperature distribution of a premixed methane flame injected at 2 m/s and attribute the instability to a Kelvin-Helmholtz instability.

The experiments and simulations investigated in the present study use a very different configuration than the previous work. Instead of studying jets, a combustible mixture, which is quiescent prior to ignition is examined. The puffing phenomenon occurs in a closed vessel that is filled entirely with a homogeneous combustible mixture and then ignited by a hot surface.

### 1.3 Thesis Outline

Results from studies on heated vessels subjected to ramp heating are presented in Chapter 2, hot surface ignition in Chapter 3, and premixed puffing flames in Chapter 4. Chapter 2 describes the experimental setup, with additional background for the diagnostic techniques presented in Appendix A and B. Experimental results are presented and discussed here with a complete list of experiments performed given in Appendix I. Additional detail of the theoretical analysis is given in Appendix C and D. Some of the thermodynamic data used in the chemical mechanism was treated for discontinuities as described in Appendix H. Chapter 3 details the dependence of ignition temperature with mixture composition and resulting flame propagation with additional literature and tabular data available in Appendix F. Experimental data and still images are available in Appendix I.2, with color images shown in Appendix L. The puffing phenomenon is described in detail in Chapter 4 with some additional scaling arguments given in Appendix G.